Solution to Electric Field Screening in Diamond Quantum Electrometers

L.M. Oberg,[1,*] M.O. de Vries,[1] L. Hanlon,[1] K. Strazdins,[1] M S.J. Barson,[1] M.W. Doherty,[1,†] and J. Wrachtrup[2]

[1] *Laser Physics Center, Research School of Physics, Australian National University, Australian Capital Territory 2601, Australia*

[2] *3rd Institute of Physics, University of Stuttgart and Institute for Quantum Science and Technology (IQST), Pfaffenwaldring 57, Stuttgart D-70569, Germany*

(Received 22 December 2019; revised 18 March 2020; accepted 12 May 2020; published 28 July 2020)

There are diverse interdisciplinary applications for nanoscale-resolution electrometry of elementary charges under ambient conditions. These include characterization of two-dimensional electronics, charge transfer in biological systems, and measurement of fundamental physical phenomena. The nitrogen-vacancy center in diamond is uniquely capable of such measurements, however electrometry thus far has been limited to charges within the same diamond lattice. It has been hypothesized that the failure to detect charges external to diamond is due to quenching and surface screening, but no proof, model, or design to overcome this has yet been proposed. In this work we affirm this hypothesis through a comprehensive theoretical model of screening and quenching within a diamond electrometer and propose a solution using controlled nitrogen doping and a fluorine-terminated surface. We conclude that successful implementation requires further work to engineer diamond surfaces with lower surface-defect concentrations.

DOI: 10.1103/PhysRevApplied.14.014085

I. INTRODUCTION

Nanoscale charge imaging has been employed for diverse purposes including high-sensitivity biological and chemical sensors [1,2], detectors within quantum devices [3], and investigating fundamental physical phenomena [4,5]. Many techniques have been employed for precision electrometry with nanometer spatial resolution [4–7], elementary charge detection [4,5,8–14], and the ability to operate at ambient temperatures and pressures [12,14]. However, no device yet possesses all three of these properties simultaneously. This capability would be extremely valuable for investigating biological systems, such as neurons [15], and as a critical characterization tool for the emerging field of two-dimensional electronics [16–18]. For example, atomic resolution imaging of silicene to aid development of a room-temperature transistor [19], probing charged quasiparticles in MOS_2 films [20], and detection of polarization skyrmions [21].

The nitrogen-vacancy (N-V) center [22] is currently the only system capable of nanoscale-resolution electrometry of elementary charges under ambient conditions. This point defect in diamond consists of a substitutional nitrogen atom (N_S) situated adjacent to a carbon vacancy. Single N-V centers have demonstrated room-temperature a.c. (d.c.) electric field sensitivities reaching 202 V cm^{-1} Hz$^{-1/2}$ (891 V cm^{-1} Hz$^{-1/2}$) [23,24]. Ensembles of N-V centers have achieved shot-noise-limited ac sensitivities on the order of 1 V cm^{-1} Hz$^{-1/2}$ [25] and have also been employed as *in situ* electric field sensors within semiconductor heterojunctions [26].

The N-V center's proficiency for quantum sensing is due to a unique combination of capabilities. Firstly, the N-V exhibits bright optical fluorescence allowing for identification of single defects that can be employed for measurements with nanoscale resolution. Secondly, the N-V possesses a mechanism for optical spin initialization and readout which permits spin resonances of individual defects to be measured with high fidelity [22]. Finally, the N-V boasts the longest room-temperature coherence time for any solid-state defect [27] allowing for high-resolution detection of spin resonances when combined with optical readout. In addition to electrometry these properties have been applied for precision nanomagnetometry [28–31], thermometry [32–34] and quantum computing [35–38] and error correction [39], as well as proposed for investigating fundamental physical phenomena such as magnetic phase changes [40] and coherent quantum transport [41].

While the N-V center can exist in several charge states, including neutral (N-V^0) and negative (N-V^-), only the latter possesses the aforementioned properties needed for electrometry [22]. In particular, the spin resonances of the N-V^- triplet ground state are susceptible to electric-field-induced changes in its electron spin-spin interactions. The resulting Stark shifts can be detected using optically

*lachlan.oberg@anu.edu.au
†marcus.doherty@anu.edu.au

detected magnetic resonance (ODMR) and used to determine the field magnitude. This is achieved through application of a strong magnetic field transverse to the N-V spin axis. The resulting N-V spin-resonance frequencies are then found to be linearly susceptible to both axial and transverse electric fields as per [24]

$$f_{\pm} \approx f_{\pm}(0) + k_z E_z \mp k_{\perp} E_{\perp} \cos(2\phi_B + \phi_E), \qquad (1)$$

where the N-V axis is denoted by z, $k_z = 0.035\,\mathrm{kHz\,m/V}$ and $k_{\perp} = 1.7\,\mathrm{kHz\,m/V}$ are the electric susceptibility parameters [42], $\tan\phi_B = B_y/B_x$, $\tan\phi_E = E_y/E_x$, $B_{\perp} = \sqrt{B_x^2 + B_y^2}$, $E_{\perp} = \sqrt{E_x^2 + E_y^2}$ and $f_{\pm}(0)$ are the resonance frequencies in the absence of an electric field (which have dependence on $B_{\perp}$ but not on ϕ_B). Additionally, Eq. (1) demonstrates that vector components of the electric field can be measured through rotation of the bias transverse magnetic field [24].

Although single N-V centers possess sufficiently high sensitivities, elementary charges external to diamond have not been detected with nanoscale resolution. We hypothesize that this is because of electric field screening and charge-state quenching of N-V centers. For the former, recent experimental works have identified multiple screening sources inherent to diamond systems. These include Debye screening from bulk defects [43], charge reorganization in primal sp^2 surface defects [44] and polarization of adsorbed water vapor [45]. Moreover, p-type defects within bulk diamond [46], surface acceptor defects [44], and surface terminations with negative electron affinities [47] are known to quench the negative charge state, particularly for near-surface N-V centers [48,49]. However, the extent that these sources impact charge detection are unknown, and a comprehensive theoretical treatment is needed.

The first aim of this paper is to develop a physical model of screening due to the external environment, internal diamond, and diamond surface. This is performed in Sec. II where we identify that screening due to charge rearrangement amongst sp^2 surface defects is the greatest impediment to electrometry. We propose a solution by saturating the charge traps through a sacrificial δ-doped layer of N_S. The effectiveness of this idea is explored in Sec. III in which an analytical toy model is developed for a simplified electrometer. Finally, in Sec. IV this toy model is adapted into a more sophisticated device compatible with N-V quantum sensing. The electrostatic properties of the device are modeled computationally, and the physical parameters optimized for charge detection. We conclude that this design successfully mitigates screening for concentrations of sp^2 surface defects below approximately $10^{16}\ \mathrm{m}^{-2}$, two orders of magnitude lower than that currently demonstrated on fluorine-passivated diamond [44].

II. SCREENING AND QUENCHING WITHIN DIAMOND

The sources and effects of screening and quenching within diamond can be considered individually within three coupled subsystems; the external atmosphere, the surface, and the internal diamond. These three environments and their associated screening and quenching sources are depicted in Fig. 1. In the following subsections we model each system individually and assess the associated impacts for diamond electrometry.

A. External atmosphere

We first address screening due to the external atmosphere at ambient temperature and pressure. As air possesses a relative permittivity of approximately unity it causes negligible electrical screening. In contrast, the physisorption of water vapor on the diamond surface may be a detrimental source of screening given water's high relative permittivity. This subsection reviews the current understanding of wetting on diamond surfaces and applies these results to form a cohesive theory of screening due to water adsorption.

Considering the most common diamond surface terminations, oxygen is known to be strongly hydrophilic and therefore not suitable for precision electrometry [54]. While hydrogen-terminated surfaces exhibit polar

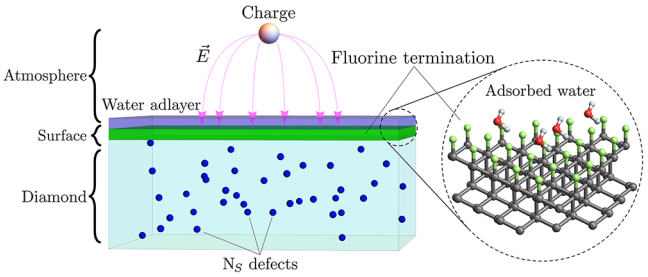

FIG. 1. Schematic of the three-layered model used to investigate field screening and N-V^- charge quenching. The external environment contains the ambient atmosphere and the charge distribution to be detected. Water vapor adsorbs to the diamond surface to form an adlayer which causes dielectric screening. This can be mitigated by passivating the diamond with fluorine, which exhibits strong dipolar hydrophobicity [50,51]. Furthermore, fluorine-terminated diamond is chemically inert, room-temperature stable, and possesses a positive electron affinity [52]. While a (111) surface termination is depicted here, other fluorinated diamond geometries possess similar desirable properties. The surface itself contains a high density of sp^2 surface defects which introduce acceptor levels into the diamond band structure [44]. These readily quench the N-V^- charge state and at partial occupation lead to strong surface-screening effects. Within the diamond, uncontrolled doping of n-type defects such as N_S lead to Debye screening [53].

hydrophobicity [45,50], they are not viable for electrometry with near-surface N-V centers. This is because they possess a negative electron affinity, which introduces subsurface holes that quench the N-V^- charge state [47]. However, this is not the case for fluorine-terminated diamond, which is chemically inert and room-temperature stable [48] with a positive electron affinity [52]. Importantly, the fluorine surface exhibits strong hydrophobicity [51,54], reflected by its high wetting angle and a small physisorption energy of 0.07 eV for F-C(111) as determined using *ab initio* calculations [50]. Ideally these adsorption energies could be used in conjunction with a suitable isotherm equation to determine the water coverage. Unfortunately, this is not possible as current studies neglect Gibbs contributions to adsorption and so cannot accurately predict coverages under ambient conditions.

Regardless, it can be expected that surface coverage is much lower than a monolayer. Simple analysis with the Brunauer-Emmett-Teller isotherm indicates negligible coverage as the condensation energy of water far exceeds that of physisorption (neglecting entropic and enthalpic contributions) [55]. Furthermore, we note that in general wetting behavior on hydrophobic surfaces is complicated. Graphene templating in conjunction with atomic force microscopy has revealed the formation of complex water structures on a range of hydrophobic surfaces, including the accumulation of nanodroplets on surface defects and step edges [56]. While we are unaware of any studies focusing explicitly on fluorine-terminated diamond surfaces, it is possible that similar behavior also exists.

We now investigate whether adsorbed water produces a major or minor screening effect. Given the ambiguity of the nature and extent of wetting on hydrophobic diamond surfaces, we model the dielectric permittivity as a function of adsorbed water adlayers. This is denoted by θ, the fractional amount of water monolayers adsorbed on the surface between 0 and 1. While surface-adsorbed vapor likely possesses a high rate of diffusion at room temperature, here we only consider the time-averaged response of the induced permittivity. For the purpose of these calculations we consider wetting on the F-C(111) surface because its electrical properties have been well-characterized theoretically [50]. However, we expect that these results are applicable to other cuts of fluorine-terminated diamond surfaces and note that (111) diamond is not explicitly required for electrometry.

The polar C-F surface bonds induce an electric field, which orientates the dipoles of the physisorbed water. This generates a net polarization in the direction of the C-F dipoles, which can be calculated at thermal equilibrium. The polarization density is given by [57]

$$\vec{P}(\vec{E}_s) = \mu\mathcal{N}\mathcal{L}(\beta\mu|\vec{E}_s|)\hat{E}_s, \tag{2}$$

where $\mu = 1.85$ D is the dipole moment of water, $\beta = (k_B T)^{-1}$, $\vec{E}_s$ is the electric field generated by the diamond surface, $\mathcal{N}$ the number density of water molecules and $\mathcal{L}(x)$ the Langevin function given by

$$\mathcal{L}(x) = \coth(x) - \frac{1}{x}.$$

A value for $\mathcal{N}$ may be estimated by treating each F as a single adsorption site. This is justified as *ab initio* calculations indicate that the energy of a physisorbed H_2O molecule is minimized when aligned laterally with a terminating F atom [50]. In the direction perpendicular to the surface (denoted $\hat{z}$) the linear density of water molecules are bound by that of liquid water, yielding $\mathcal{N} = 0.156 \times \theta$ molecules/Å^3.

We now consider the electrostatic response of the dipolar water layer to some perturbing field generated by the charged source, $\vec{E}_p$. Denoting the electric field generated by the C-F surface dipoles as $\vec{E}_s = E_s\hat{z}$, the total electric field can be written as

$$\vec{E} = \vec{E}_s + \vec{E}_p.$$

The polarization of the water layer due to $\vec{E}_p$ can be characterized through a first-order Taylor expansion of Eq. (2) about $\vec{E}_s$ as

$$\vec{P}(\vec{E}_s + \vec{E}_p) = \vec{P}(\vec{E}_s) + \epsilon_0 \overleftrightarrow{\chi}(\vec{E}_s) \cdot \vec{E}_p, \tag{3}$$

where $\overleftrightarrow{\chi}$ is the linear electric susceptibility tensor given by

$$\begin{aligned}
\epsilon_0 \overleftrightarrow{\chi}_{i,j}(\vec{E}_s) &= \left.\frac{d\vec{P}_i}{d\vec{E}_{p,j}}\right|_{\vec{E}_s} \\
&= \mu\mathcal{N}\left[\left.\frac{d\mathcal{L}_i}{dE_{p,j}}\right|_{\vec{E}_s}\hat{E}_s + \mathcal{L}(\beta E_s)\frac{d\hat{E}_{s,i}}{dE_{p,j}}\right] \\
&= \mu\mathcal{N}\left[\beta\left(\frac{1}{\beta^2 E_s^2} - \operatorname{csch}^2(\beta E_s)\right)\delta_{i,z}\right. \\
&\quad \left. + \frac{\mathcal{L}(\beta E_s)}{E_s}\delta_{i,j}\right].
\end{aligned}$$

Consequently, $\overleftrightarrow{\chi}$ may be written as the sum of an isotropic (χ_0) and anisotropic (χ_1) component as

$$\overleftrightarrow{\chi} = \chi_0 \overleftrightarrow{\mathbb{I}} + \chi_1\hat{z}\hat{z}, \tag{4}$$

where

$$\begin{aligned}
\epsilon_0\chi_0 &= \frac{\mu\mathcal{N}\mathcal{L}(\beta E_s)}{E_s}, \\
\epsilon_0\chi_1 &= \mu\mathcal{N}\beta\left(\frac{1}{\beta^2 E_s^2} - \operatorname{csch}^2(\beta E_s)\right) - \epsilon_0\chi_0.
\end{aligned}$$

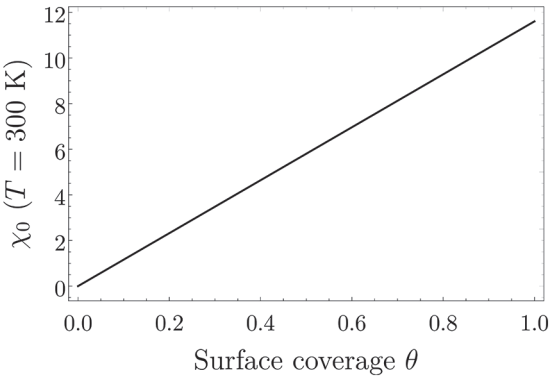

FIG. 2. Isotropic susceptibility of a water adlayer physisorbed on fluorine-terminated diamond as a function of surface coverage at 300 K.

Therefore, the change in polarization of the adlayer induced by $\vec{E}_p$ is given by

$$\Delta\vec{P} = \epsilon_0 \overleftrightarrow{\chi} \cdot \vec{E}_p = \epsilon_0 \chi_0 \vec{E}_p + \epsilon_0 \chi_1 \vec{E}_{p,z}\hat{z}. \tag{5}$$

Taking $E_s \sim 0.1$ V/Å derived from *ab initio* calculations [50], we find that $\chi_1 \ll \chi_0$ at 300 K and therefore the anisotropic term may be neglected. The isotropic susceptibility is presented as a linear function of surface coverage in Fig. 2 where we obtain $\chi_0 \approx 12$ for $\theta = 1$. The susceptibility of the water adlayer is therefore relatively large but diminished in respect to liquid water. This is because the ability of the adlayer molecules to reorientate in response to an electric field is constrained by the surface. In the following section these susceptibilities are used to model the screening ratio due to both the water adlayer and bulk diamond.

B. Defects within bulk diamond

Debye screening due to internal defects presents a major impediment to diamond electrometry. Also referred to as Thomas-Fermi screening, this effect is a linear approximation of the well-known band-bending phenomenon and occurs when charges are free to rearrange within a spatial continuum of donors and acceptors [53]. This causes external fields to decay exponentially within the lattice as they are counteracted by the induced response of the charges. Within diamond, electrons are free to reorganize themselves amongst uncontrolled defects. For example, the uncontrolled presence of substitutional N defects produces a common and potent source of Debye screening with a characteristic decay length of 15 nm at low doping concentrations [43]. In addition to screening, p-type defects such as boron are detrimental to electrometry as they introduce holes which quench the N-V^- center [46]. Consequently, only pure diamond is compatible with precision electrometry in which isotropic polarizability is the sole source of internal field decay.

Ignoring presently the impact of surface defects, the magnitude of screening due to the adsorbed water layer and pure diamond can be determined analytically. As depicted in the inset of Fig. 3, a basic electrometer may be modeled by three stacked planar dielectrics consisting of a thin water layer sandwiched between diamond and air. If an elementary charge is placed above the surface, the electrostatic problem can be solved using the method of images [58,59]. This technique solves Poisson's equation by introducing an infinite series of fictitious "image" charges, which reproduce the boundary conditions of the dielectric stack.

In Fig. 3 we present the electric field screening ratio of a point charge located at varying heights above the surface. The screening ratio represents the magnitude of the screened field relative to the unscreened field. In this case we sample at a depth of 10 nm into the lattice, corresponding to a possible location of a near-surface N-V center. A lower estimate for the thickness of the water layer is taken to be 3 Å, approximately the van der Waals radius of a single H_2O molecule. We obtain screening ratios of approximately 0.3, independent of surface coverage and the height of the charge above the surface. This is comparable to the screening ratio purely due to the dielectric response of diamond and indicates that adsorption of water vapor is not detrimental to nanoscale electrometry. While a 70% reduction in the unscreened field strength appears considerable, this is unavoidable, and minor compared

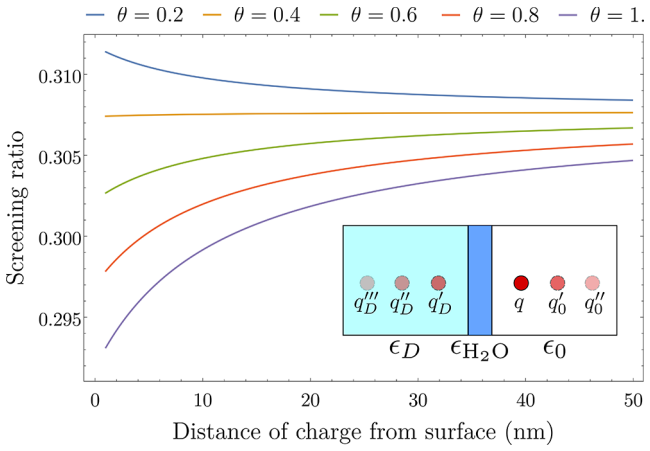

FIG. 3. Electric field screening ratio at a depth of 10 nm into diamond for varying water-surface coverage. This represents the ratio of the screened field magnitude relative to the unscreened field magnitude (i.e., within a vacuum) produced by a point charge (q). In this model the water layer is 3 Å wide. The inset depicts the method of images used to determine the screening ratio. Here fictitious "image" charges (dashed qs) are introduced to solve Poisson's equation. The magnitude of the charges and their positions are such that they reproduce the electrostatic boundary conditions of the three stacked dielectrics, representing the diamond, water adlayer, and external atmosphere.

to screening induced by surface-charge rearrangement as discussed below.

C. Surface

Uncontrolled, diamond-surface defects present a detrimental source of screening and charge quenching for N-V-based electrometers. Recent work has identified a family of primal sp^2 defects common to many widely used diamond-surface terminations [44]. These introduce acceptor states into diamond approximately 2.2 eV above the valence band which readily quench the N-V^- charge state at 2.9 eV [60]. Furthermore, partial occupation of these traps results in intense field screening through permitting unimpeded rearrangement of surface charge. For F-C(100), an sp^2 surface trap density of 4% has been observed following passivation using SF_6 plasma [44], corresponding to a trap concentration of roughly 10^{18} m^{-2}. We are unaware of surface-trap concentrations present on diamond geometries other than (100) and acknowledge that they may be in excess of 10^{18} m^{-2}. We therefore consider 10^{18} m^{-2} as the current threshold for trap concentrations on all F-terminated diamond surfaces.

In principle vector electrometry can be performed regardless of diamond orientation. However, referring to Eq. (1), we have that $k_\perp > k_z$ and hence it is sensible to favor a particular geometry depending on the charge distribution being detected. For example, one would obtain the greatest ODMR sensitivity when detecting an external point charge with a (110) diamond geometry. While the N-V orientation does provide a geometric advantage, we demonstrate in Sec. II that control of surface defects is the critical factor for successful electrometry in any realistic device.

III. TOY-MODEL ELECTROMETER

A solution to both surface-induced screening and charge instability is to saturate the surface traps using sacrificial donors within the diamond. We propose fabricating a δ-doped layer of N_S, which introduces a donor level 3.8 eV above the valence band. In the limit that the concentration of N_S exceeds that of the sp^2 defects, the Fermi level will be pinned to the donor level and prevent quenching of the N-V^-. This is possible as present doping techniques allow for precision control of the δ-layer height and defect concentrations up to 1000 ppm [49,61]. In this section we demonstrate the effectiveness of this idea through an analytical toy model that explores the complex interactions of screening and quenching within a highly coupled system.

Consider the schematic for a simplified electrometer presented in Fig. 4(a). The δ-doped layer is positioned at a depth D below the diamond surface ($z = 0$) while the N-V spin probe is placed between them at a depth $d < D$. At electrostatic equilibrium the occupation of the sp^2 defects leads to the accumulation of an isotropic and homogeneous

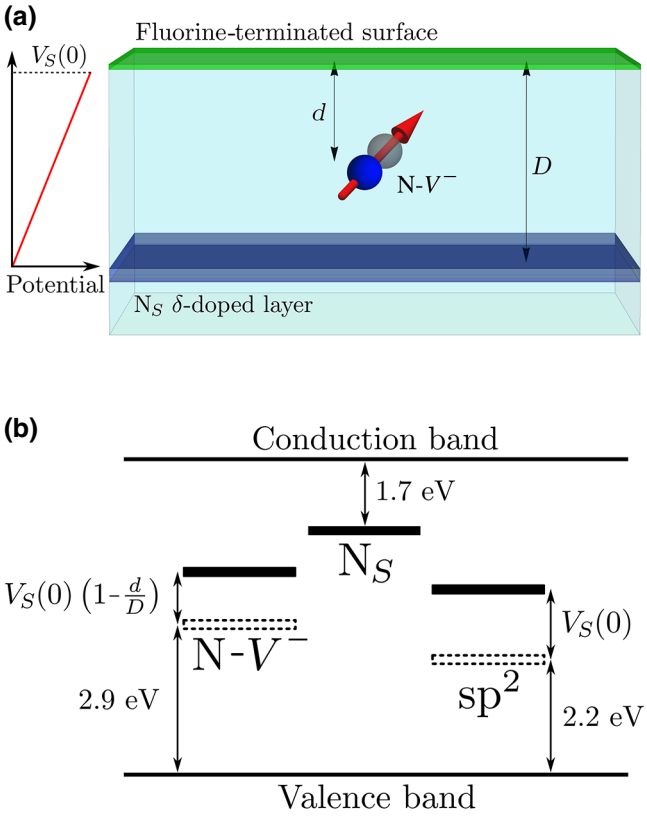

FIG. 4. (a) Schematic of the toy-model electrometer. An N-V center (nitrogen represented as the blue sphere, vacancy as the gray sphere, and ground-state spin as the red arrow) is positioned a depth d below a fluorine-terminated surface. A (100) diamond geometry is depicted. The surface possesses a density σ_T of sp^2 charge traps, which are preferentially saturated by a grounded N_S δ-doped layer positioned at a depth D. This generates a negative charge density at the surface subsequently forming a parallel plate capacitor. A linear potential extends throughout the capacitor with a magnitude $V_S(0)$ at the surface. (b) Energy-level diagram of defect states within the diamond electrometer. The acceptor level of the sp^2 charge traps is raised by an energy $V_S(0)$, while that of the N-V center is raised by $V_S(0)\,(1 - d/D)$. Charge stability of the N-V^- center requires full occupation of the charge traps and $E_{\text{N-}V} + V_S(0)\,(1 - d/D) \ll E_N$.

charge density on the surface, ρ_S. This charge density subsequently generates a surface potential $V_S(z = 0)$, which is related as per

$$\rho_S = CV_S(0) = q\sigma_T f\,(E_T + qV_S(0) - E_N), \qquad (6)$$

where C is the device capacitance, q is the electron charge, σ_T is the density of surface traps, f is the Fermi-Dirac distribution, $E_N = 3.8$ eV is the energy of N_S and $E_T \approx 2.2$ eV is the energy of an sp^2 surface defect [44]. The two layers—surface and δ doping—effectively form a parallel plate capacitor and hence $C = \epsilon_D/D$ where $\epsilon_D = 5.7\epsilon_0$ is the dielectric permittivity of diamond. This induces a linear potential between the capacitor plates such that the

potential at the N-V center is given by

$$V_S(d) = V_S(0)\left(1 - \frac{d}{D}\right). \tag{7}$$

The magnitude of the potential induced at the surface has major ramifications for N-V^- charge stability. Figure 4(b) depicts the energies of N_S, N-V, and sp^2 defects within the simplified electrometer. Upon charging, the sp^2 defect and N-V energies are raised by an amount $qV_S(0)$ and $qV_S(d)$, respectively. To avoid transition to N-V^0, the condition

$$E_{\text{N-}V} + qV_S(d) \ll E_N, \tag{8}$$

must be maintained. Inserting Eq. (7) into the inequality (8) places a constraint on the maximum surface potential that prevents quenching, given by

$$qV_S(0) \ll \frac{E_N - E_{\text{N-}V}}{\left(1 - \frac{d}{D}\right)}. \tag{9}$$

The surface potential also has major implications for screening. Note that $V_S(0)$ is ultimately limited above by $0 \leq qV_S(0) \leq E_N - E_T \approx 1.6$ eV. When $qV_S(0) \approx E_N - E_T$ the defect energy is pinned to that of the N_S donors and screening effects dominate; equation (6) indicates that $\rho_S = q\sigma_T/2$ and hence the surface is effectively conducting. Clearly, electrometry requires that

$$qV_S(0) \ll E_N - E_T \tag{10}$$

for under such conditions $f\,(E_T + qV_S(0) - E_N) \approx 1$ (the linear regime) and the surface charge cannot reorganize in response to an external electric field. Fortunately, the inequality (10) can be determined precisely and the robustness of the linear regime to charge screening can be demonstrated quantitatively.

Consider the screening field induced by a perturbing potential at the diamond surface, δV. Within the linear regime we have that

$$\begin{aligned}\rho_S &= q\sigma_T f\,(E_T + q[V_S(0) + \delta V] - E_N),\\ &= q\sigma_T f\,(\Delta + q\delta V),\\ &\approx q\sigma_T\left(1 - q\beta e^{\beta\Delta}\delta V\right),\end{aligned} \tag{11}$$

where we denote $\Delta \equiv [E_T + qV_S(0) - E_N]$ and expand to first order in δV. Suppose that the perturbing potential is due to a point charge Q positioned a height h above the electrometer surface and aligned with the N-V center. Then Eq. (11) indicates that the induced charge density is given by

$$\begin{aligned}\delta\rho_S(r) &= -q^2\sigma_T\beta e^{\beta\Delta}\delta V,\\ &= -\frac{q^2 Q\sigma_T\beta e^{\beta\Delta}}{4\pi\epsilon_0\sqrt{h^2 + r^2}},\end{aligned} \tag{12}$$

as a function of radial distance from the point charge r. This produces a screening field at the N-V center given by

$$\begin{aligned}\delta E(d) &= \frac{\hat{z}}{2\epsilon_0}\int_0^\infty \delta\rho_S(r)\frac{d}{(d^2 + r^2)^{3/2}}rdr,\\ &= -\frac{q^2 Q\sigma_T\beta e^{\beta\Delta}}{8\pi\epsilon_0^2(d + h)}\hat{z}.\end{aligned} \tag{13}$$

Considering that the field generated by the point charge at a depth d in the absence of screening is

$$E(d) = \frac{Q}{4\pi\epsilon_0}\frac{\hat{z}}{(d + h)^2}, \tag{14}$$

the screening ratio as a function of d is given by

$$R = \left|\frac{E(d) + \delta E(d)}{E(d)}\right| = 1 - \frac{q^2\sigma_T\beta e^{\beta\Delta}(d + h)}{2\epsilon_0}. \tag{15}$$

Equation 15 demonstrates a further bound on the maximum surface potential compatible with electrometry. Taking $(d + h) = 200$ nm and $\sigma_T = 10^{18}$ m^{-2} we obtain a screening ratio of $R \approx 1 - 10^{-22}e^{\beta qV_S(0)}$. Surface screening will render electrometry impossible if the surface potential is not sufficiently deep within the linear regime of the Fermi-Dirac distribution. In this specific example, a ratio $R \geq 99\%$ only occurs for $qV_S(0) \leq 1.19$ eV $\approx E_N - E_T - 16k_BT$ at room temperature.

To summarize, our toy model has identified the fundamental limitations to precision electrometry. The potential of the surface must be controlled such that all charge traps are saturated while the N-V energy is maintained below the Fermi level. In general, one should aim to reduce $V_S(0)$ to avoid the detrimental effects of screening and quenching. Equation (6) indicates that the surface potential is a function of only two variables; the capacitance and the density of charge traps. For the simplified electrometer design, $V_S(0) \propto C^{-1}$ within the linear regime and therefore D should be minimized. However, D is limited below by physical constraints such as the thickness of the δ-doped layer and its proximity to the surface and N-V center. Hence the surface potential is largely dictated by the density of surface traps. Whereas the capacitance can be controlled, surface defects are an undesirable byproduct of diamond-surface passivation [44].

The performance of a diamond electrometer is strongly dependent on the surface-trap density. This relationship is

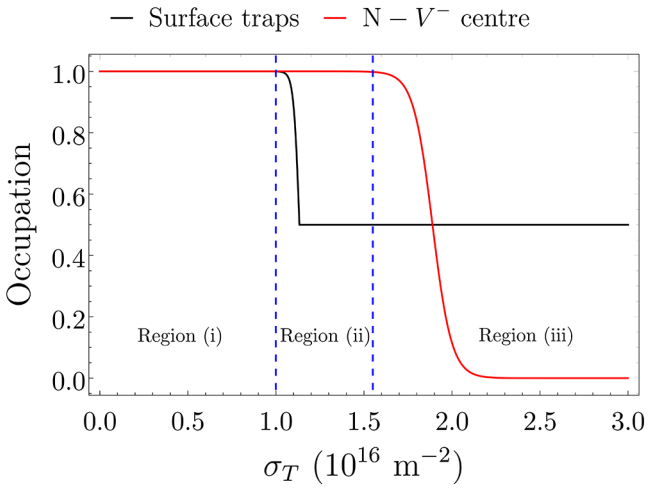

FIG. 5. Occupation of surface traps and the N-V^- charge state as a function of surface-trap density for the toy-model electrometer. Here we assume that $D = 100$ nm, $d = 60$ nm, and $T = 300$ K. Three different electrometer operational regions have been distinguished and are discussed in the text.

demonstrated in Fig. 5, where we invert Eq. (6) to determine $V_S(0)$ as a function of σ_T. This allows us to determine the occupation of both the surface traps and N-V^- center as a function of trap concentration through their respective Fermi-Dirac distributions. We choose $D = 100$ nm, $d = 60$ nm, and $T = 300$ K as a realistic example of device parameters. Three different electrometer operating regions can be distinguished. Region (i) represents values of σ_T, which correspond to surface voltages within the linear regime. Here electrometry is viable as the charge traps are fully saturated and the N-V maintains its negative charge state. Region (ii) also represents values of σ_T for which the N-V^- center remains charge stable. However, the sp^2 defects are only partially occupied and so electrometry is impossible due to surface screening. Similarly, in region (iii) σ_T is so large that the N-V center has been quenched.

Consequently, the presence of a N_S δ-doped layer can simultaneously maintain N-V^- stability and prevent surface screening within the linear regime. However, the capabilities of the device are fundamentally limited by the density of surface traps. As capacitance is a geometric property, Eq. (6) indicates that this result is universal to any device that employs donors to saturate surface defects. The parallel plate capacitor has one of the greatest capacitances over small length scales and hence Fig. 5 demonstrates that electrometry is only compatible with surface densities on the order of $\sigma_T \lesssim 10^{16}$ m^{-2}. This is two orders of magnitude lower than defect densities currently observed on fluorine-terminated surfaces passivated using SF_6 plasma. However, fluorine is a relatively new surface termination and many alternative passivation techniques exist and continue to be developed [48,52,62]. The sp^2 defect yields on these surfaces are yet to be characterized and may well be low enough to permit precision electrometry.

IV. ELECTROMETER DESIGN

Beyond the detrimental effects of surface screening, the simple electrometer presented in the previous section has several deficiencies, which make it impractical for quantum sensing. Fortunately, these can be overcome with a simple modification to the electrometer design. In this section we discuss the shortcomings of the toy-model electrometer and their solutions, culminating in the presentation of an effective and physically realizable device. This device is then modeled computationally to determine which surface-trap densities are compatible with electrometry. In doing so, we establish a benchmark required for surface-passivation technologies before nanoscale charge sensing is viable.

Initialization and readout of the N-V center requires optical control using a green laser (approximately 532 nm) [22–24]. As depicted in Fig. 6, performing electrometry with the toy device requires the optical path to pass through the δ-doped N_S layer. This introduces several complications. Firstly, N_S layers typically contain some density of erroneous N-V centers. These are capable of producing background counts during readout which decrease measurement contrast and lead to lower sensitivity. Secondly, the green laser also ionizes N_S defects to form N_S^+ which modulates the charge density within the δ-doped layer [63]. During the optical steady state this results in a local positive potential, which may reduce charge stability of the N-V^- center and further diminishes signal contrast.

Moreover, following initialization of the N-V^- spin state, the laser is deactivated and the induced charge relaxes back to the equilibrium it adopted before the laser was turned on. If this relaxation time is slow (approximately 100 ns) compared to the N-V sensing period ($>$ 1 μs) [23,24], this relaxation will influence the sensing measurement. Ionization of N_S also introduces free charge carriers into the lattice, and hence there also exists a low probability of Auger electrons scattering against the N-V^- and causing quenching. Finally, the δ-doped N_S layer acts as a spin bath, which can cause decoherence of the N-V spin at close proximities [64].

The extent to which erroneous N photoionization influences N-V electrometry is unknown. This requires a complex model of electron drift diffusion dependent on the internal field of the electrometer. Moreover, this must be coupled with the effects of interelectron repulsion, retrapping by N_S, N-V charge-state dynamics, and finally how the resulting charge distribution influences N-V spin. Successful implementation also requires a variety of key parameters, which are currently unknown, such as electron trapping cross sections, and will therefore be addressed in future works.

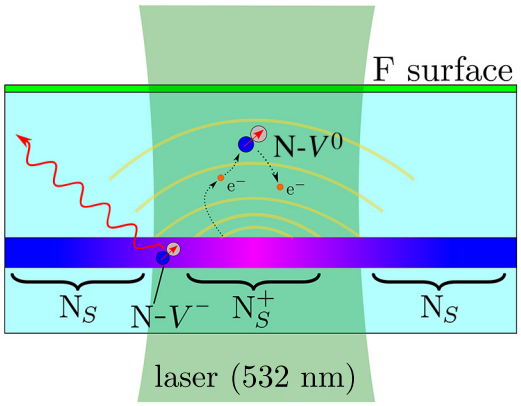

FIG. 6. Screening and quenching mechanisms induced by ionization of N_S during optical control of the N-V center. The laser (532 nm) induces a density of N_S^+ defects within the δ-doped layer (depicted in pink), which subsequently generates a local positive potential (yellow contour lines) and ionizes free electrons into the lattice (orange circles). The local potential has the potential to reduce N-V^- charge stability while the modulating charge density interferes with N-V spin dynamics during quantum sensing. There is also a lower risk of N-V^- charge destabilization due to scattering with Auger electrons. Erroneous N-V centers present in the doped layer can also introduce background counts during readout (red photon) which increases measurement contrast leading to lower sensitivity.

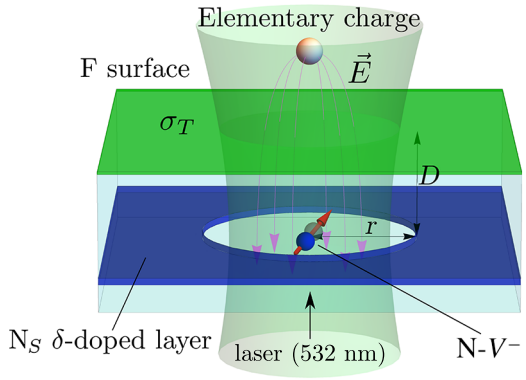

FIG. 7. Schematic of a diamond-based electrometer for subnanometer-resolution charge imaging at ambient temperatures. A shallow N-V^- spin probe detects the electric field from an elementary charge positioned above the surface through optically detected magnetic resonance. Primal sp^2 defects present on the surface with density σ_T act as electron traps, quenching the N-V^- charge state and causing detrimental screening when partially occupied. This is systematically controlled by saturating the charge traps using a sacrificial layer of δ-doped N_S positioned a depth D into the substrate. A N_S-deficit disk of radius r allows for optical initialization and readout of the N-V^- without ionizing mobile charge carriers from the δ-doped layer. The laser (532 nm) is incident from beneath the electrometer opposite of the sensing side.

Alternatively, one possible solution to these issues is to spatially separate the N_S layer and the N-V center. The optical focus can then be maintained on the N-V while the δ doping is subject to a negligible laser intensity. We estimate this would require a separation distance of approximately 0.5 μm. However, this severely limits the sensitivity of the spin probe to external charges as Eq. (9) necessitates that $D \gtrsim 1$ μm and therefore $d \gtrsim 0.5$ μm to maintain N-V^- charge stability. A more practical solution is to introduce a hole within the δ-doped layer. Consider the schematic presented in Fig. 7 in which a disk of pure diamond is fabricated around the N-V center. This hole permits optical access to the spin probe while simultaneously minimizing the number of ionized N_S defects. Furthermore, the hole reduces the probability of optically addressing multiple N-V centers and so increases the yield of electrometer fabrication. We note that we are unaware of any similar implementations of δ-layer templating in diamond, however we believe it is feasible using currently existing nanofabrication technology. For example, one possibility may be to mill the desired geometry using reactive ion etching [65] followed by overgrowth using conventional chemical vapor deposition [66].

The capabilities of this realistic electrometer design for elementary charge detection are investigated using COMSOL Multiphysics software. The potential at the N-V center and surface as well as the occupation of charge traps are simulated as a function of the device parameters; the N-V depth d, N_S layer depth D, and hole radius r. This is achieved by solving Poisson's equation self-consistently for a surface charge density given by Eq. (6) and assuming a grounded δ-doped layer. The device parameters are then optimized to identify the greatest possible trap density compatible with precision electrometry. As discussed in Sec. III, these criterion are charge stability of the N-V [$qV_S(d) \ll E_N - E_{\text{N-}V} = 0.9$ eV] and a surface potential that produces a screening ratio in excess of 99% as per Eq. (15).

Figure 8 presents the largest viable surface-trap density as a function of the δ-doping depth and hole radius. Trap densities greater than those presented lead to field screening in excess of 1% of the unscreened field. For the parameters sampled here (30 nm $< D <$ 100 nm and 80 nm $< r <$ 150 nm) we find that electrometry is feasible for sp^2 surface densities within the regime of 10^{15} m^{-2} and that no charge quenching occurs for N-V centers level with the δ-doped layer. Devices with smaller radii and δ-doping depth possess a greater capacitance and are therefore compatible with larger defect densities. Note that the optical spot size is diffraction limited by approximately 200 nm, and hence some degree of N_S ionization may occur for hole radii less than approximately 100 nm. Regardless, if the effects are significantly detrimental, Fig. 8 indicates that the hole size can simply be increased beyond the

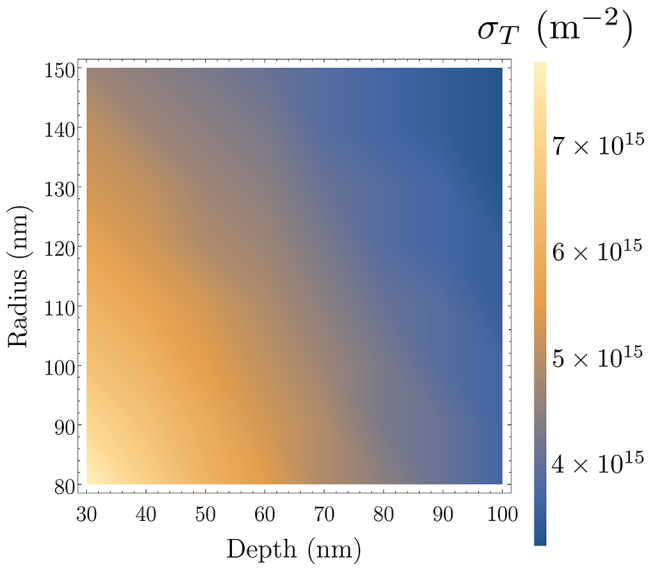

FIG. 8. Maximum viable surface-trap density (σ_T) as a function of δ-doped N_S layer depth and hole radius for the electrometer design presented in Fig. 7. Trap densities in excess of those presented here result in an electric field screening ratio lower than 99% (i.e., the field is screened greater than 1% of its unscreened value).

optical spot size without drastically reducing the achievable sp^2 defect concentrations. For example, if the radius is increased to 200 nm the viable surface-trap concentration is still limited above by approximately 10^{15} m^{-2}. If these hole dimensions are still insufficient to mitigate the effects of erroneous N photoionization, the laser wavelength can be increased up to 575 nm (corresponding to the N-V^0 excitation energy of 2.156 eV) without significantly reducing N-V^- charge stability or the capacity for spin polarization [22]. This results in at least a 100-fold reduction of the N photoionization cross section [67].

V. CONCLUSION

Subnanometer resolution electrometry of elementary charges under ambient conditions allow for investigation of diverse electrical phenomenon ranging from biological systems to fundamental physics. The N-V center is the only known system capable of such a feat, however measurements are currently limited to charges internal to diamond. In this paper we apply theoretical modeling to conclusively demonstrate that external charge detection is not yet feasible due to field screening. While screening due to the atmosphere and internal defects can be mitigated using fluorine-passivated and ultrapure diamond, electrometry is ultimately frustrated by charge rearrangement amongst surface defects.

We propose a solution to surface screening through introduction of a sacrificial N_S δ-doped layer. Fabrication of a N_S deficit hole surrounding the N-V center allows for optical access to the spin probe while minimizing the readout of erroneous N-V centers and ionization of free charges. This electrometry device is technologically feasible and computational simulations demonstrate that it can successfully mitigate screening effects for surface-trap densities up to approximately 10^{16} m^{-2}. Although this is 2 orders of magnitude below currently observed sp^2 defect densities on fluorine-terminated diamond, the outcome of this work is a clear pathway towards nanoscale imaging of external charges at ambient conditions. Electrometry cannot be achieved until surface passivation technologies realize lower defect concentrations on fluorine-terminated diamond.

ACKNOWLEDGMENTS

We acknowledge funding from the Australian Research Council (DP170102735). We thank Patrick Maletinsky for providing insightful feedback on this paper.

[1] Y. Cui, Q. Wei, H. Park, and C. M. Lieber, Nanowire nanosensors for highly sensitive and selective detection of biological and chemical species, Science **293**, 1289 (2001).
[2] F. Patolsky, G. Zheng, and C. M. Lieber, Fabrication of silicon nanowire devices for ultrasensitive, label-free, real-time detection of biological and chemical species, Nat. Protoc. **1**, 1711 (2006).
[3] J. M. Eizerman, R. Hanson, L. H. Van Beveren, B. Witkamp, L. M. Vandersypen, and L. P. Kouwenhoven, Single-shot read-out of an individual electron spin in a quantum dot, Nature **430**, 431 (2004).
[4] J. Martin, N. Akerman, G. Ulbricht, T. Lohmann, J. H. Smet, K. Von Klitzing, and A. Yacoby, Observation of electron-hole puddles in graphene using a scanning single-electron transistor, Nat. Phys. **4**, 144 (2008).
[5] M. J. Yoo, T. A. Fulton, H. F. Hess, R. L. Willett, L. N. Dunkleberger, R. J. Chichester, L. N. Pfeiffer, and K. W. West, Scanning single-electron transistor microscopy: Imaging individual charges, Science **276**, 579 (1997).
[6] A. K. Henning, T. Hochwitz, J. Slinkman, J. Never, S. Hoffmann, P. Kaszuba, and C. Daghlian, Two-dimensional surface dopant profiling in silicon using scanning Kelvin probe microscopy, J. Appl. Phys. **77**, 1888 (1995).
[7] C. C. Williams, J. Slinkman, W. P. Hough, and H. K. Wickramasinghe, Lateral dopant profiling with 200 nm resolution by scanning capacitance microscopy, Appl. Phys. Lett. **55**, 1662 (1989).
[8] M. H. Devoret and R. J. Schoelkopf, Amplifying quantum signals with the single-electron transistor, Nature **406**, 1039 (2000).
[9] C. Schönenberger and S. F. Alvarado, Observation of Single Charge Carriers by Force Microscopy, Phys. Rev. Lett. **65**, 3162 (1990).
[10] Y. Martin, D. W. Abraham, and H. K. Wickramasinghe, High-resolution capacitance measurement and potentiometry by force microscopy, Appl. Phys. Lett. **52**, 1103 (1988).

[11] A. N. Cleland and M. L. Roukes, A nanometre-scale mechanical electrometer, Nature **392**, 160 (1998).
[12] J. S. Bunch, A. M. Van Der Zande, S. S. Verbridge, I. W. Frank, D. M. Tanenbaum, J. M. Parpia, H. G. Craighead, and P. L. McEuen, Electromechanical resonators from graphene sheets, Science **315**, 490 (2007).
[13] J. Salfi, I. G. Savelyev, M. Blumin, S. V. Nair, and H. E. Ruda, Direct observation of single-charge-detection capability of nanowire field-effect transistors, Nat. Nanotechnol. **5**, 737 (2010).
[14] J. Lee, Y. Zhu, and A. Seshia, Room temperature electrometry with SUB-10 electron charge resolution, J. Micromech. Microeng. **18**, 025033 (2008).
[15] L. Hanlon, V. Gautam, J. D. A. Wood, P. Reddy, M. S. J. Barson, M. Niihori, A. R. J. Silalahi, B. Corry, J. Wrachtrup, M. J. Sellars, V. R. Daria, P. Maletinsky, G. J. Stuart, and M. W. Doherty, Diamond nano-pillar arrays for quantum microscopy of neuronal signals, arXiv:1901.08743 (2019).
[16] F. Schwierz, Graphene transistors, Nat. Nanotechnol. **5**, 487 (2010).
[17] B. Radisavljevic, A. Radenovic, J. Brivio, V. Giacometti, and A. Kis, Single-layer MoS2 transistors, Nat. Nanotechnol. **6**, 147 (2011).
[18] K. F. Mak and J. Shan, Photonics and optoelectronics of 2D semiconductor transition metal dichalcogenides, Nat. Photonics **10**, 216 (2016).
[19] L. Tao, E. Cinquanta, D. Chiappe, C. Grazianetti, M. Fanciulli, M. Dubey, A. Molle, and D. Akinwande, Silicene field-effect transistors operating at room temperature, Nat. Nanotechnol. **10**, 227 (2015).
[20] K. F. Mak, K. He, C. Lee, G. H. Lee, J. Hone, T. F. Heinz, and J. Shan, Tightly bound trions in monolayer MoS2, Nat. Mater. **12**, 207 (2012).
[21] S. Das *et al.*, Observation of room-temperature polar skyrmions, Nature **568**, 368 (2019).
[22] M. W. Doherty, N. B. Manson, P. Delaney, F. Jelezko, J. Wrachtrup, and L. C. Hollenberg, The nitrogen-vacancy colour centre in diamond, Phys. Rep. **528**, 1 (2013).
[23] F. Dolde, H. Fedder, M. W. Doherty, T. Nöbauer, F. Rempp, G. Balasubramanian, T. Wolf, F. Reinhard, L. C. Hollenberg, F. Jelezko, and J. Wrachtrup, Electric-field sensing using single diamond spins, Nat. Phys. **7**, 459 (2011).
[24] F. Dolde, M. W. Doherty, J. Michl, I. Jakobi, B. Naydenov, S. Pezzagna, J. Meijer, P. Neumann, F. Jelezko, N. B. Manson, and J. Wrachtrup, Nanoscale Detection of a Single Fundamental Charge in Ambient Conditions Using the NV - Center in Diamond, Phys. Rev. Lett. **112**, 097603 (2014).
[25] E. H. Chen, H. A. Clevenson, K. A. Johnson, L. M. Pham, D. R. Englund, P. R. Hemmer, and D. A. Braje, High-sensitivity spin-based electrometry with an ensemble of nitrogen-vacancy centers in diamond, Phys. Rev. A **95**, 053417 (2017).
[26] T. Iwasaki, W. Naruki, K. Tahara, T. Makino, H. Kato, M. Ogura, D. Takeuchi, S. Yamasaki, and M. Hatano, Direct nanoscale sensing of the internal electric field in operating semiconductor devices using single electron spins, ACS Nano **11**, 1238 (2017).
[27] E. D. Herbschleb, H. Kato, Y. Maruyama, T. Danjo, T. Makino, S. Yamasaki, I. Ohki, K. Hayashi, H. Morishita, M. Fujiwara, and N. Mizuochi, Ultra-long coherence times amongst room-temperature solid-state spins, Nat. Commun. **10**, 3766 (2019).
[28] J. P. Tetienne, T. Hingant, J. V. Kim, L. Herrera Diez, J. P. Adam, K. Garcia, J. F. Roch, S. Rohart, A. Thiaville, D. Ravelosona, and V. Jacques, Nanoscale imaging and control of domain-wall hopping with a nitrogen-vacancy center microscope, Science **344**, 1366 (2014).
[29] L. Thiel, D. Rohner, M. Ganzhorn, P. Appel, E. Neu, B. Müller, R. Kleiner, D. Koelle, and P. Maletinsky, Quantitative nanoscale vortex imaging using a cryogenic quantum magnetometer, Nat. Nanotechnol. **11**, 677 (2016).
[30] T. Häberle, D. Schmid-Lorch, F. Reinhard, and J. Wrachtrup, Nanoscale nuclear magnetic imaging with chemical contrast, Nat. Nanotechnol. **10**, 125 (2015).
[31] K. Arai, C. Belthangady, H. Zhang, N. Bar-Gill, S. J. DeVience, P. Cappellaro, A. Yacoby, and R. L. Walsworth, Fourier magnetic imaging with nanoscale resolution and compressed sensing speed-up using electronic spins in diamond, Nat. Nanotechnol. **10**, 859 (2015).
[32] G. Kucsko, P. C. Maurer, N. Y. Yao, M. Kubo, H. J. Noh, P. K. Lo, H. Park, and M. D. Lukin, Nanometre-scale thermometry in a living cell, Nature **500**, 54 (2013).
[33] P. Neumann, I. Jakobi, F. Dolde, C. Burk, R. Reuter, G. Waldherr, J. Honert, T. Wolf, A. Brunner, J. H. Shim, D. Suter, H. Sumiya, J. Isoya, and J. Wrachtrup, High-precision nanoscale temperature sensing using single defects in diamond, Nano Lett. **13**, 2738 (2013).
[34] D. M. Toyli, C. F. De Las Casas, D. J. Christle, V. V. Dobrovitski, and D. D. Awschalom, Fluorescence thermometry enhanced by the quantum coherence of single spins in diamond, Proc. Natl. Acad. Sci. USA **110**, 8417 (2013).
[35] L. Childress and R. Hanson, Diamond NV centers for quantum computing and quantum networks. MRS Bulletin **38**, 134 (2013).
[36] H. Choi, M. Pant, S. Guha, and D. Englund, Percolation-based architecture for cluster state creation using photon-mediated entanglement between atomic memories, npj Quantum Inf. **5**, 104 (2019).
[37] K. Nemoto, M. Trupke, S. J. Devitt, A. M. Stephens, B. Scharfenberger, K. Buczak, T. Nöbauer, M. S. Everitt, J. Schmiedmayer, and W. J. Munro, Photonic Architecture for Scalable Quantum Information Processing in Diamond, Phys. Rev. X **4**, 31022 (2014).
[38] Y. Chen, S. Stearn, S. Vella, A. Horsley, and M. W. Doherty, Optimisation of diamond quantum processors., arXiv:2002.00545 (2020).
[39] G. Waldherr, Y. Wang, S. Zaiser, M. Jamali, T. Schulte-Herbrüggen, H. Abe, T. Ohshima, J. Isoya, J. F. Du, P. Neumann, and J. Wrachtrup, Quantum error correction in a solid-state hybrid spin register, Nature **506**, 204 (2014).
[40] J. Cai, A. Retzker, F. Jelezko, and M. B. Plenio, A large-scale quantum simulator on a diamond surface at room temperature, Nat. Phys. **9**, 168 (2013).
[41] L. M. Oberg, E. Huang, P. M. Reddy, A. Alkauskas, A. D. Greentree, J. H. Cole, N. B. Manson, C. A. Meriles, and M. W. Doherty, Spin coherent quantum transport of electrons between defects in diamond, Nanophotonics **8**, 1975 (2019).

[42] E. Van Oort and M. Glasbeek, Electric-field-induced modulation of spin echoes of N-*V* centers in diamond, Chem. Phys. Lett. **168**, 529 (1990).
[43] D. A. Broadway, N. Dontschuk, A. Tsai, S. E. Lillie, C. T.-K. Lew, J. C. McCallum, B. C. Johnson, M. W. Doherty, A. Stacey, L. C. L. Hollenberg, and J.-P. Tetienne, Spatial mapping of band bending in semiconductor devices using in situ quantum sensors, Nat. Electron. **1**, 502 (2018).
[44] A. Stacey, N. Dontschuk, J. P. Chou, D. A. Broadway, A. K. Schenk, M. J. Sear, J. P. Tetienne, A. Hoffman, S. Prawer, C. I. Pakes, A. Tadich, N. P. de Leon, A. Gali, and L. C. Hollenberg, Evidence for primal sp2 defects at the diamond surface: Candidates for electron trapping and noise sources, Adv. Mater. Interfaces **6**, 00 (2019).
[45] M. Mertens, M. Mohr, K. Brühne, H. J. Fecht, M. Łojkowski, W. Świeszkowski, and W. Łojkowski, Patterned hydrophobic and hydrophilic surfaces of ultrasmooth nanocrystalline diamond layers, Appl. Surface Sci. **390**, 526 (2016).
[46] M. Liao, Y. Koide, J. Alvarez, M. Imura, and J. P. Kleider, Persistent positive and transient absolute negative photoconductivity observed in diamond photodetectors, Phys. Rev. B – Condens. Matter Mater. Phys. **78**, 045112 (2008).
[47] M. V. Hauf, B. Grotz, B. Naydenov, M. Dankerl, S. Pezzagna, J. Meijer, F. Jelezko, J. Wrachtrup, M. Stutzmann, F. Reinhard, and J. A. Garrido, Chemical control of the charge state of nitrogen-vacancy centers in diamond, Phys. Rev. B – Condens. Matter Mater. Phys. **83**, 00 (2011).
[48] S. Cui and E. L. Hu, Increased negatively charged nitrogen-vacancy centers in fluorinated diamond, Appl. Phys. Lett. **103**, 051603 (2013).
[49] K. Ohno, F. Joseph Heremans, L. C. Bassett, B. A. Myers, D. M. Toyli, A. C. Bleszynski Jayich, C. J. Palmstrøm, and D. D. Awschalom, Engineering shallow spins in diamond with nitrogen delta-doping, Appl. Phys. Lett. **101**, 082413 (2012).
[50] L. Mayrhofer, G. Moras, N. Mulakaluri, S. Rajagopalan, P. A. Stevens, and M. Moseler, Fluorine-terminated diamond surfaces as dense dipole lattices: The electrostatic origin of polar hydrophobicity, J. Am. Chem. Soc. **138**, 4018 (2016).
[51] E. Kissa, *Fluorinated Surfactants and Repellents* (CRC Press, New York, 2001), 2nd ed., Vol. 97.
[52] K. J. Rietwyk, S. L. Wong, L. Cao, K. M. Odonnell, L. Ley, A. T. Wee, and C. I. Pakes, Work function and electron affinity of the fluorine-terminated (100) diamond surface, Appl. Phys. Lett. **102**, 091604 (2013).
[53] B. K. Ridley, *Quantum Processes in Semiconductors* (Oxford University Press, New York, 2013), 5th ed.
[54] C. J. Widmann, C. Giese, M. Wolfer, S. Kono, and C. E. Nebel, F-and Cl-terminations of (100) oriented single crystalline diamond, Phys. Status Solidi (A) Appl. Mater. Sci. **211**, 2328 (2014).
[55] S. Brunauer, P. H. Emmett, and E. Teller, Adsorption of gases in multimolecular layers, J. Am. Chem. Soc. **60**, 309 (1938).
[56] P. Cao, K. Xu, J. O. Varghese, and J. R. Heath, The microscopic structure of adsorbed water on hydrophobic surfaces under ambient conditions, Nano Lett. **11**, 5581 (2011).
[57] P. Atkins and J. de Paula, *Atkins' Physical Chemistry* (Oxford University Press, Oxford, 2014), 10th revis ed.
[58] R. G. Barrera, O. Guzmán, and B. Balaguer, Point charge in a three-dielectric medium with planar interfaces, Am. J. Phys. **46**, 1172 (1978).
[59] F. M. Pont and P. Serra, Comment on point charge in a three-dielectric medium with planar interfaces [Am. J. Phys. 46, 1172–1179 (1978)], Am. J. Phys. **83**, 475 (2015).
[60] N. Aslam, G. Waldherr, P. Neumann, F. Jelezko, and J. Wrachtrup, Photo-induced ionization dynamics of the nitrogen vacancy defect in diamond investigated by single-shot charge state detection, New J. Phys. **15**, 013064 (2013).
[61] M. Chandran, S. Michaelson, C. Saguy, and A. Hoffman, Fabrication of a nanometer thick nitrogen delta doped layer at the sub-surface region of (100) diamond, Appl. Phys. Lett. **109**, 221602 (2016).
[62] M. C. Salvadori, W. W. Araújo, F. S. Teixeira, M. Cattani, A. Pasquarelli, E. M. Oks, and I. G. Brown, Termination of diamond surfaces with hydrogen, oxygen and fluorine using a small, simple plasma gun, Diamond Relat. Mater. **19**, 324 (2010).
[63] K. Iakoubovskii and G. J. Adriaenssens, Optical transitions at the substitutional nitrogen centre in diamond, J. Phys. Condens. Matter **12**, L77 (2000).
[64] G. Balasubramanian, P. Neumann, D. Twitchen, M. Markham, R. Kolesov, N. Mizuochi, J. Isoya, J. Achard, J. Beck, J. Tissler, V. Jacques, P. R. Hemmer, F. Jelezko, and J. Wrachtrup, Ultralong spin coherence time in isotopically engineered diamond, Nat. Mater. **8**, 383 (2009).
[65] Y. Ando, Y. Nishibayashi, K. Kobashi, T. Hirao, and K. Oura, Smooth and high-rate reactive ion etching of diamond, Diamond Relat. Mater. **11**, 824 (2002).
[66] J. E. Butler, Y. A. Mankelevich, A. Cheesman, M. Jie, and M. N. R. Ashfold, Understanding the chemical vapor deposition of diamond: Recent progress, J. Phys.: Condens. Matter **21**, 364201 (2009).
[67] J. Isberg, A. Tajani, and D. J. Twitchen, Photoionization measurement of deep defects in single-crystalline CVD diamond using the transient-current technique, Phys. Rev. B – Condens. Matter Mater. Phys. **73**, 245207 (2006).